# The facile oil-phase synthesis of a multi-site synergistic high-entropy alloy to promote the alkaline hydrogen evolution reaction

Dan Zhang,[a,b,#] Yue Shi,[a,#] Huan Zhao,[a] Wenjing Qi,[d] Xilei Chen,[b] Tianrong Zhan,[a] Shaoxiang Li,[b] Bo Yang,[b] Mingzi Sun,[c] Jianping Lai,[a]* Bolong Huang,[c]* and Lei Wang[a,b]*

Although intensive efforts and great progress have been achieved in electrocatalytic hydrogen evolution reaction (HER), the advanced synthesis strategy of efficient electrocatalyst is still the most significant goal. In this paper, we introduce the PdFeCoNiCu high-entropy alloy (HEAs) nanoparticles (NPs) as an efficient electrocatalyst for HER, which has been prepared in the oil phase at the facile condition for the first time. PdFeCoNiCu/C shows excellent alkaline HER catalytic performance with an overpotential of only 18 mV, Tafel slope of 39 mV $dec^{-1}$. Meanwhile, we achieved the highest mass activity in alkaline HER among all non-Pt electrocatalysts. PdFeCoNiCu/C also showed surprisingly stable catalytic properties for over 15 days without notable decay. Based on theoretical calculations, the HEA surface demonstrates the optimization of electronic structures based on the synergistic effect of all metals. The Pd and Co are confirmed to be the dominant electroactive sites for both $H_2$ formation and initial water splitting, which are guaranteed by the promotion of Ni, Fe and Cu for the enhanced electron transfer and optimized the binding energy of hydrogen intermediates. This work has supplied a significant insight into the design of efficient electrocatalyst based on HEA materials.

## Introduction

Hydrogen evolution reaction (HER) of the cathode in the electrolytic cell can effectively convert the electric energy generated by solar and wind energy into chemical energy.[1-10] As we all know, Pt/C is currently recognized as the best HER catalyst. However, Pt resource is scarce and expensive, and it lacks the ability to promote water splitting under alkaline conditions, so there is still much room for improvement in alkaline HER.[11-18] Moreover, the stability of Pt/C is not good enough, and it is easy to decay prematurely during the electrolysis process.[19,20] According to our previous research, it was found that Pd can effectively promote the water splitting process under alkaline conditions and promote HER.[21] However, the catalytic kinetics and stability of Pd-based materials are still inadequate throughout the whole reaction progress.[22-24]

In addition, the continuous emergence of new materials has also injected fresh blood into electrocatalysis. Through precisely controlling the coordination entropy, high-entropy alloys (HEAs) are synthesized from five or more metal elements with the same atomic ratio.[25,26] Research has proved that HEAs exhibit distinctive properties such as extremely strong mechanical strength and corrosion resistance under severe conditions.[27] These unique characteristics are due to the high

[a]*Key Laboratory of Eco-chemical Engineering, Key Laboratory of Optic-electric Sensing and Analytical Chemistry of Life Science, Taishan Scholar Advantage and Characteristic Discipline Team of Eco Chemical Process and Technology, College of Chemistry and Molecular Engineering, Qingdao University of Science and Technology, Qingdao 266042, P. R. China.*
[b]*Shandong Engineering Research Center for Marine Environment Corrosion and Safety Protection, College of Environment and Safety Engineering, Qingdao University of Science and Technology, Qingdao 266042, P. R. China*
[c]*Department of Applied Biology and Chemical Technology, the Hong Kong Polytechnic University, Hung Hom, Kowloon, Hong Kong SAR, China*
[d] *College of Chemistry, Chongqing Normal University, Chongqing 401331, P. R. China.*
[#]*Equal Contribution*
Correspondence *E-mail:* inorchemwl@126.com, bhuang@polyu.edu.hk, jplai@qust.edu.cn.
Electronic Supplementary Information (ESI) available: [details of any supplementary information available should be included here]. See DOI: 10.1039/x0xx00000x

entropy effect caused by the lattice distortion and slow diffusion as the number of components increases.[28] In the catalytic process, alloying can significantly adjust the adsorption energy of molecules and intermediates on the catalyst surface, thereby enhancing its catalytic activity. However, prior methods of synthesizing HEAs include arc melting method, carbothermal shock method, melt spinning method, aerosol spray pyrolysis method, ball milling method and solvothermal method, etc.[29-33] Nevertheless, these methods not only often produce nanoparticles (NPs) with large average size and irregular morphology but also face challenges such as complicated process, high processing coast, or low yield. In addition, these processes often require high-temperature and high-pressure conditions. These limitations have hindered the practical usage of HEAs in various applications.

In this paper, a Pd-based HEA PdFeCoNiCu nanoparticles (PdFeCoNiCu NPs) was successfully obtained under low temperature (≤ 250°C) and atmospheric pressure with small size (~34 nm) in oil phase for the first time and applied to the alkaline electrocatalytic HER. Nano-sized alloy particles increased the specific surface area of the electrocatalyst, and when combined with Ketchen Black, it has a larger contact area, which exposed more active sites in the alkaline HER. According to the experimental results, the mass activity reached 6.51 A $mg^{-1}_{Pd}$ at -0.07 V *vs.* RHE. The overpotential is 18 mV at 10 mA $cm^{-2}$. It is the non-Pt electrocatalyst with the highest mass activity in alkaline HER so far, even more than most Pt-based catalysts (**Table S2**). Subsequently, its stability was explored. After 15 days of uninterrupted testing, its catalytic activity remained in its original state and its structure remained intact. From the DFT calculations, the optimal balance of the electronic structures between metals on the HEA surface has been confirmed. The flexible Ni sites are bifunctional in promoting both proton and OH stabilization to Pd and Co sites. Both Cu and Fe are essential in stabilizing the electroactivity and the morphology.

**Results and Discussions**

The PdFeCoNiCu HEA NPs were synthesized by a one-step route. In a typical synthesis method, $Pd(acac)_2$, $Co(acac)_3$, $Fe(acac)_3$, $Cu(acac)_2$, $Ni(acac)_2$ and $Mo(CO)_6$ were added into oleylamine in a vial, sonicated for 30 min. The solution was heated to 220 °C from room temperature under magnetic stirring and held for 2 h. Then the final black gelatinous products were collected by centrifugation and stored in cyclohexane for further us. In the synthesis process, oleylamine and carbonyl may play an important role in coordination and merge with different metal ions. The morphology of PdFeCoNiCu NPs was characterized by transmission electron microscopy (TEM). Synthesized NPs are uniformly in size **(Fig. 1a)**. **Fig. 1b** displays the size distribution details of the PdFeCoNiCu NPs, and the size distribution is relatively balanced. The high-resolution TEM micrograph (HRTEM) can clearly see the lattice fringes **(Fig. 1c)**, corresponding to 0.204 nm (111). TEM-mapping (**Fig. 1e**) shows that the five metals of Pd, Fe, Co, Ni, Cu are located on the surface of the nanoparticles. The above characterizations proved that the synthesis of PdFeCoNiCu NPs was successful. Inductively coupled plasma atomic emission spectroscopy (ICP-AES) was explored the composition of the PdFeCoNiCu NPs, closed to Pd:Fe:Co:Ni:Cu ≈ 19:21:20:22:17 (**Table S1**), which matched the EDX image of PdFeCoNiCu NPs (**Fig. S1**). The XRD pattern of the PdFeCoNiCu NPs is shown in **Fig. 1d**. Since the FeNi content ratio is higher in the PdFeCoNiCu NPs, the measured XRD matches the JCPDS NO. 38-0419. As **Fig. 1d** indicates, there is a strong

diffraction peak at ~44.1°, which is ascribed to the body-centered cubic (BCC) (111). The diffraction peaks of (220) and (200) are extremely weak, which proved that the (111) crystal plane dominates in the PdFeCoNiCu NPs, and the diffraction peak of (111) is slightly wide duo to the small size of the synthesized PdFeCoNiCu NPs and mixing in nanometer level structure.[34,35]

In order to explore the valence states of Pd, Fe, Co, Ni and Cu, X-ray photoelectron spectroscopy (XPS) testing was performed (**Fig. S2**). At the same time, the XPS found that the content ratio of Pd:Fe:Co:Ni:Cu is 18.3:23.1:21.0:21.3:16.3, which is basically consistent with the ICP-AES test data, which further proves the successful preparation of HEAs. $Pd^0$ $3d_{5/2}$ of $Pd^0$ $3d_{3/2}$ are concentrated at 335.1 eV and 340.5 eV, respectively (**Fig. S2a)**; for Fe $2p_{3/2}$, 709.4 eV is attributed to $Fe^0$, the peaks around 714.8 eV belong to the high valence state of $Fe^{3+}$. The peaks around 722.6 eV and 724.0 eV belong to $Fe^0$ $2p_{1/2}$ and $Fe^{3+}$ $2p_{1/2}$ respectively (**Fig. S2b)**; for Co 2p, 778.3 eV and 793.3 eV belong to $Co^0$ $2p_{3/2}$ and $Co^0$ $2p_{1/2}$, 783.0 eV and 798.0 eV belong to $Co^{2+}$ $2p_{3/2}$ and$Co^{2+}$ $2p_{1/2}$ (**Fig. S2c)**. **Fig. S2d** shows $2p_{3/2}$ of $Ni^0$ and $Ni^{2+}$, and two peaks correspond to 853.3 eV and 855.2 eV respectively, the peaks around 870.2 eV and 874.4 eV belong to the $2p_{1/2}$ of $Ni^0$ and $Ni^{2+}$. **Fig. S2e** shows that Cu belongs to $Cu^0$, the two peaks are located in sections 932.6 eV and 952.5 eV.
Subsequently, by combining PdFeCoNiCu NPs with Ketjen black to form PdFeCoNiCu/C (**Fig. S3**) electrocatalyst of 1 mg $mL^{-1}$. PdFeCoNiCu/C was placed in 1.0 M KOH electrolyte and tested the HER properties using a three-electrode system. In order to highlight the superiority of hydrogen evolution activity of PdFeCoNiCu/C, we compared it with Pd/C and commercial Pt/C catalysts. The polarization curves (**Fig. 2a)** indicate that the initial potential of PdFeCoNiCu/C is very minor, and the overpotential at 10 mA $cm^{-2}$ is only 18 mV (**Fig. 2b**), which is 5 times less than Pt/C (91 mV), compared to Pd/C (418 mV), improved 400 mV. The hydrogen evolution activity of PdFeCoNiCu/C was also evaluated by mass activity **(Fig. 2c&S4)**, at -0.07 V *vs.* RHE, the mass activity of PdFeCoNiCu/C reached 6.51 A $mg^{-1}_{Pd}$, while Pt/C is only 0.65 A $mg^{-1}_{Pt}$. In addition, the Tafel slope is also the lowest of these materials (**Fig. 2d**). Impedance can explore the interfacial properties of the catalyst, and smaller impedances can also increase the activity of PdFeCoNiCu/C (**Fig. S5**). At the same time, PdFeCoNiCu/C has a large electrochemical double layer capacitance (EDLC) (**Fig. S6**), indicating that PdFeCoNiCu/C has a higher electrochemical active area. When the overpotential is 200 mV, the TOF of Pt/C and the PdFeCoNiCu/C achieves 2.23 $s^{-1}$ and 3.13 $s^{-1}$ respectively (**Fig. S7**). Gas chromatography was used to detect the hydrogen produced during the reaction progress, and the relationship between the hydrogen yield and time shows a perfect linear relationship, and the result consistent with the theoretical hydrogen production. Faraday efficiency is close to 100% (**Fig. S8**).

Furthermore, the catalytic stability of PdFeCoNiCu/C was evaluated by the CV cycle, the long-term current versus time curve and the voltage versus time curve. The attenuation trend of the polarization curves before and after the test is completely negligible (**Fig. 3a**). Then, the relationship between current and time (I-t) was tested (**Fig. 3b**). After 15 days, the attenuation of the current density was negligible. We compared the voltage-time curves of Pt/C and PdFeCoNiCu/C. It can be clearly found that the Pt/C voltage is significantly more attenuated than PdFeCoNiCu/C at the current density of 10 mA $cm^{-2}$ (**Fig. S9**). In summary, PdFeCoNiCu/C has excellent stability. The

catalyst after the stability test was characterized by TEM (**Fig. S10a**), XRD (**Fig. S10b**) and HRTEM (**Fig. S10c**). The PdFeCoNiCu/C after the reaction did not fall off from the carbon material, and there was no difference from the pre-reaction. However, Pt/C showed obvious agglomeration (**Fig. S11**). XRD also represents that it still has good crystallinity.

The HER performance of HEAs under the alkaline environment has been studied in detail. For the HEA structures, the surface distortion was observed, especially near the Cu sites, forming the step-like surface structure. The induced surface strain further leads to the surface electronic modulation. The surface-active bonding and anti-bonding orbitals near the Fermi level ($E_F$) have been located near Co and Ni sites, indicating the potential electroactive sites for the initial water splitting effect for HER in the alkaline environment (**Fig. 4a-4b**). The projected density of states (PDOSs) of the HER surfaces has been demonstrated to illustrate the local electronic environment. Pd and Cu sites have shown the electron-rich feature, both locating near Ev-2.5 eV. The broad Fe-3d band has been noticed with evident $e_g$ and $t_{2g}$ splitting. Ni-3d has shown a sharp peak at Ev-1.0 eV while Co-3d shows the evident crossing of $E_F$ with high electron density, which supports the high electroactivity for both Ni and Co sites (**Fig. 4c**). The further detailed studies of the site-dependent PDOSs of each element in HEA are illustrated to compare their individual role in promoting HER performance. From surface to bulk sites, an obvious shift towards the lower position has been noticed for Pd-4d orbitals, supporting the enhanced electroactive adsorption of the freely migrate proton during HER performance. Moving from the bulk Fe to the surface Fe sites, the $e_g$-$t_{2g}$ gap slightly alleviates to enhance the *d-d* electron coupling, which compensates the electrons at the nearby Co-sites to preserve the high electroactivity during the HER process. With the protection by Fe sites, the Co-3d band center has been pinned at Ev-1.6 eV from bulk to surface, which plays as the main electron-depletion center to dissociate the adsorbed water. The Ni sites with the highest concentration have shown a gradually merged 3d-band from the bulk to the surface, accompanying the upwards shifting of the band center. The intermediate position of the Ni-3d band plays as the flexible booster for both H and $H_2O$ splitting of nearby Pd and Co sites, respectively. The electron-rich Cu also shift towards the $E_F$ to promote the holistic electron transfer between metal sites (**Fig. S12**). For the key adsorption of the initial reactant $H_2O$, the strong *p-d* coupling is noticed due to the 1.48 eV downshifting of *s,p* bands by water adsorption, guaranteeing the sufficient supply of proton for HER (**Fig. S13a**). Meanwhile, we further noticed the efficient p-d couplings of *OH with Co and Ni sites, indicating the efficient water-splitting and stable adsorption of *OH, which play as the double insurance for the superior HER performance (**Fig. S13b**). For the free migrating H*, the small gap between H-1s and Pd-4d bands benefits the fast Tafel reaction of $H_{ads}$ combination for $H_2$ generation (**Fig. S13c**).

The most stable structural configurations of the reactants and key intermediates adsorption are demonstrated. The stable adsorption of $H_2O$ is located on Co sites while the nearby Ni facilitates the OH stabilization from water splitting. For the proton capture for HER, the facilitation of Ni to the Pd sites is also noted, which is consistent with the electronic structures. The desorption of the formed $H_2$ is noticed near the Pd sites (**Fig. 4d**). From the energetic view, the alkaline HER on the HEA surface shows a continuous downhill trend with the total energy releasement of 1.37 eV, supporting a stronger physicochemical trend of alkaline HER as experiment observations (**Fig. 4e**).

More importantly, the HEA surface shows small activation energy of 0.21 eV for water-splitting, confirming the energetically favorable water-splitting process, which contributes to the remarkable HER performance in the alkaline media (**Fig. 4f**). Therefore, theoretical calculations of the HEA shows the synergistic effect of the five metal elements in optimizing the electronic environment to achieve satisfied HER performance.

## Conclusions

In summary, the PdFeCoNiCu HEA NPs were successfully prepared for the first time in the oil phase at low temperature (≤ 250 °C) and atmospheric pressure. The electrocatalytic properties of the PdFeCoNiCu HEA NPs show that the mass activity of PdFeCoNiCu/C reached 6.51 A $mg^{-1}_{Pd}$ at -0.07 V *vs*. RHE, and the overpotential is only 18 mV (10 mA $cm^{-2}$) for the alkaline HER, which exceeds the mass activity of all the reported non-Pt catalyst. In addition, the surprising stability of PdFeCoNiCu/C is another unique feature. Even after half a month of uninterrupted testing, there was no sign of decline in the electroactivity. And the structure of the electrocatalyst has been well preserved. DFT calculations have revealed the significant role of each metal component in the HEA for realizing the superior HER performance. Fe enhances the d-d electron coupling and compensates the electrons at the Co position, thereby maintaining high electrical activity during the HER process. Electron-rich Cu promotes overall electron transfer between metal sites. The pinning of electroactive Co sites for water-splitting while the nearby Ni facilitates the *OH stabilization from water splitting. And highly active Pd sites for $H_2$ formation determine the efficient HER process in the alkaline media. This works not only supplied the simple low-temperature oil phase synthesis method for realizing the large-scale production of HEAs in the future but also opens a promising direction for designing highly efficient alkaline HER catalysts.

## Conflicts of interest

There are no conflicts to declare.


## Acknowledgements

This work was supported by the National Natural Science Foundation of China (51772162, 51802171, 21771156), the Taishan Scholars Program, Natural Science Foundation of Shandong Province, China (ZR2018BB031), Youth Innovation of Shandong Higher Education Institutions, China (2019KJC004), Outstanding Youth Foundation of Shandong Province, China (ZR2019JQ14), the Taishan Scholar Project of Shandong Province (tsqn201909123) and and the Early Career Scheme (ECS) fund (Grant No.: PolyU 253026/16P) from the Research Grant Council (RGC) in Hong Kong.


## Notes and references


1. J. Zhu, L. Hu, P. Zhao, L. Y. S. Lee, K.-Y. Wong, *Chem. Rev.*, 2020, **120**, 851-918.
2. Y. Zheng, Y. Jiao, M. Jaroniec, S. Z. Qiao, *Angew. Chem. Int. Ed.*, 2015, **54**, 52-65
3. Y. Xu, M. Kraft, R. Xu, *Chem. Soc. Rev.*, 2016, **45**, 3039-3052.

4. X. F. Lu, L. Yu, J. Zhang, X. W. Lou, *Adv. Mater.*, 2019, **31**, 1900699.
5. P. Yu, F. Wang, T. A. Shifa, X. Zhan, X. F. Xia, J. He, *Nano Energy*, 2019, **58**, 244-276.
6. S.-Y. Bae, J. Mahmood, I.-Y. Jeon, J.-B. Baek, *Nanoscale Horiz.*, 2019, **4**, 43-56.
7. X.-K. Wan, H. B. Wu, B. Y. Guan, D. Luan, X. W. Lou, *Adv. Mater.*, 2020, **32**, 1901349.
8. Y. Zhao, T. Ling, S. Chen, B. Jin, A. Vasileff, Y. Jiao, L. Song, J. Luo, S. Qiao, *Angew. Chem. Int. Ed.*, 2019, **58**, 12252-12257.
9. N. Yao, P. Li, Z. Zhou, Y. Zhao, G. Cheng, S. Chen, W. Luo, *Adv. Energy Mater.*, 2019, **9**, 1902449.
10. D. Zhao, K. Sun, W.-C. Cheong, L. Zheng, C. Zhang, S. Liu, X. Cao, K. Wu, Y. Pan, Z. Zhuang, B. Hu, D. Wang, Q. Peng, C. Chen, Y. Li, *Angew. Chem. Int. Ed.*, 2019, **59**, 8982-8990.
11. Y. Li, X. Tan, R. K. Hocking, X. Bo, H. Ren, B. Johannessen, S. C. Smith, C. Zhao, *Nat. Commun.*, 2020, **11**, 2720.
12. J.-X. Feng, S.-Y. Tong, Y.-X. Tong, G.-R. Li, *J. Am. Chem. Soc.*, 2018, **140**, 5118-5126.
13. Y.-W. Peng, C. Shan, H.-J. Wang, L.-Y. Hong, S. Yao, R.-J. Wu, Z.-M. Zhang, T.-B. Lu, *Adv. Energy. Mater.*, 2019, **9**, 1900597.
14. J. Wang, F. Xu, H. Jin, Y. Chen, Y. Wang, *Adv. Mater.*, 2017, **29**, 1605838.
15. J.-Q. Chi, X.-J. Zeng, X. Shang, B. Dong, Y.-M. Chai, C.-G. Liu, M. Marin, Y. Yin, *Adv. Funct. Mater.*, 2019, **29**, 1901790.
16. L. Dai, Z.-N. Chen, L. Li, P. Yin, Z. Liu, H. Zhang, *Adv. Mater.*, 2020, **32**, 1906915.
17. D. Zhang, H. Mou, F. Lu, C. Song, D. Wang, *Appl. Catal. B: Environ.*, 2019, **54**, 471-478.
18. J. Lai, B. Huang, Y. Chao, X. Chen, S. Guo, *Adv. Mater.*, 2019, **31**, 1805541.
19. Z. Pu, I. S. Amiinu, Z. Kou, W. Li, S. Mu, *Angew. Chem. Int. Ed.*, 2017, **56**, 11559-11564.
20. J. Yin, J. Jing, H. Zhang, M. Lu, Y. Peng, B. L. Huang, P. X. P. Xi, C.-H. Yan, *Angew. Chem. Int. Ed.*, 2019, **58**, 18676-18682.
21. D. Zhang, H. Zhao, B. Huang, B. Li, H. Li, Y. Han, Z. Wang, X. Wu, Y. Pan, Y. Sun, X. Sun, J. Lai, L. Wang, *ACS Cent. Sci.*, 2019, **5**, 1991-1997.
22. J. Fan, X. Cui, S. Yu, L. Gu, Q. Zhang, F. Meng, Z. Peng, L. Ma, J.-Y. Ma, K. Qi, Q. Bao, W. Zheng, *ACS Nano*, 2019, **13**, 12987-12995.
23. R.-Q. Yao, Y.-T. Zhou, H. Shi, Q.-H. Zhang, L. Gu, Z. Wen, X.-Y. Lang, Q. Jiang, *ACS Energy Lett.*, 2019, **4**, 1379-1386.
24. T. Bhowmik, M. K. Kundu, S. Barman, *ACS Catal.*, 2016, **6**, 1929-1941.
25. E. P. George, D. Raabe, R. O. Ritchie, *Nat. Rev. Mater.*, 2019, **4**, 515-534.
26. X. Chang, M. Zeng, K. Liu, L. Fu, *Adv. Mater.*, 2020, **32**, 1907226.
27. Y. Yao, Z. Liu, P. Xie, Z. Huang, T. Li, D. Morris, Z. Finfrock, J. Zhou, M. Jiao, J. Gao, Y. Mao, J. Miao, P. Zhang, R. Shahbazian-Yassar, C. Wang, G. Wang, L. Hu, *Sci. Adv.*, 2020, **6**, eaaz0510.
28. G. R. M. Tomboc, T. Kwon, J. Joo, K. Lee, *J. Mater. Chem. A.*, 2020, **8**, 14844-14862.
29. M. Bondesgaard, N. L. N. Broge, A. Mamakhel, B. B. Iversen, *Adv. Funct. Mater.*, 2019, **29**, 1905933.
30. Y.G. Yao, Z. N. Huang, P. F. Xie, S. D. Lacey, R. J. Jacob, H. Xie, F. J. Chen, A. M. Nie, T. C. Pu, M. Rehwoldt, D. W. Dai, M. R. Zachariah, C. Wang, S. Y. Reza, J. Li, L. B. Hu, *Science*, 2018, **359**, 1489-1494.
31. Z. F. Lei, X. J. Liu, Y. Wu, H. Wang, S. H. Jiang, S. D. Wang, X. D. Hui, Y. D. Wu, B. Gault, P. Kontis, D. Raabe, L. Gu, Q. H. Zhang, H. W. Chen, H. T. Wang, J. B. Liu, K. An, Q. S. Zeng, T.-G. Nieh, Z. P. Lu, *Nature*, 2018, **563**, 546-550.

32. Z. Y. Jin, J. Lv, H. L. Jia, W. H. Liu, H. L. Li, Z. H. Chen, X. Lin, G. Q. Xie, X. J. Liu, S. H. Sun, H. J. Qiu, *Small*, 2019, **15**, 1904180.
33. X. Z. Wang, Z. N. Huang, Y. G. Yao, H. Y. Qiao, G. Zhong, Y. Pei, C. L. Zheng, D. Kline, Q. Q. Xia, Z. W. Lin, J. Q. Dai, M. R. Zachariah, B. Yang, S. Y. Reza, L. B. Hu, *Mater. Today*, 2020, **35**, 106-114.
34. W. Zhang, Y. Yang, B. Huang, F. Lv, K. Wang, N. Li, M. Luo, Y. Chao, Y. Li, Y. Sun, Z. Xu, Y. Qin, W. Yang, J. Zhou, Y. Du, D. Su, S. Guo, *Adv. Mater*., 2019, **31**, 1805833.
35. K. Jiang, D. Zhao, S. Guo, X. Zhang, X. Zhu, J. Guo, G. Lu, X. Huang, *Sci. Adv.*, 2017, **3**, e1601705.

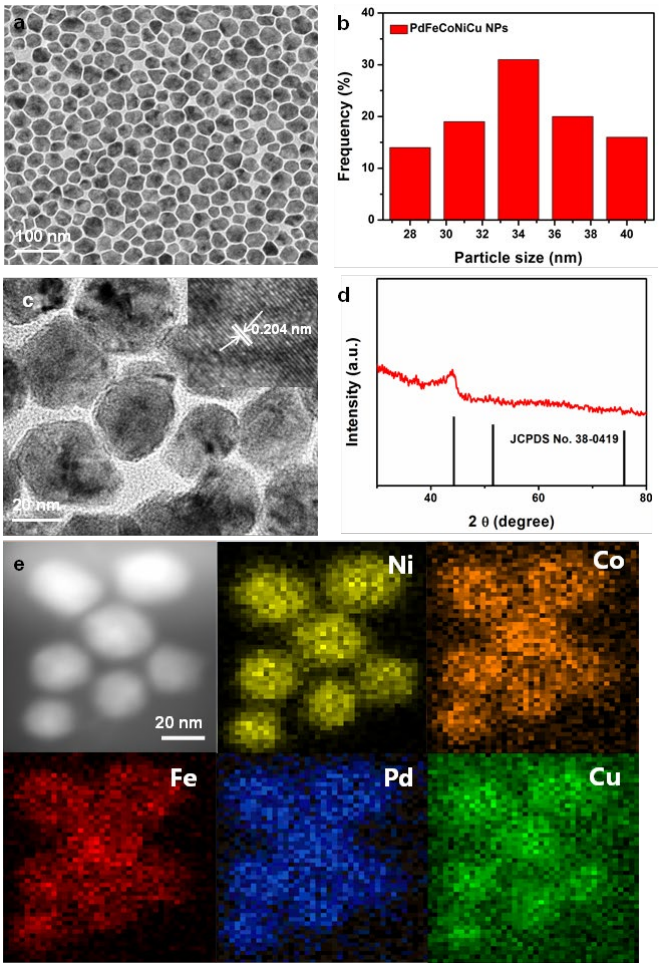


**Fig. 1** (a) XRD pattern of PdFeCoNiCu NPs. (b) TEM and (c) HRTEM images of PdFeCoNiCu NPs (the lattice fringes insert). (d) Size distribution of PdFeCoNiCu NPs. (e) The corresponding TEM elemental mapping of PdFeCoNiCu NPs.

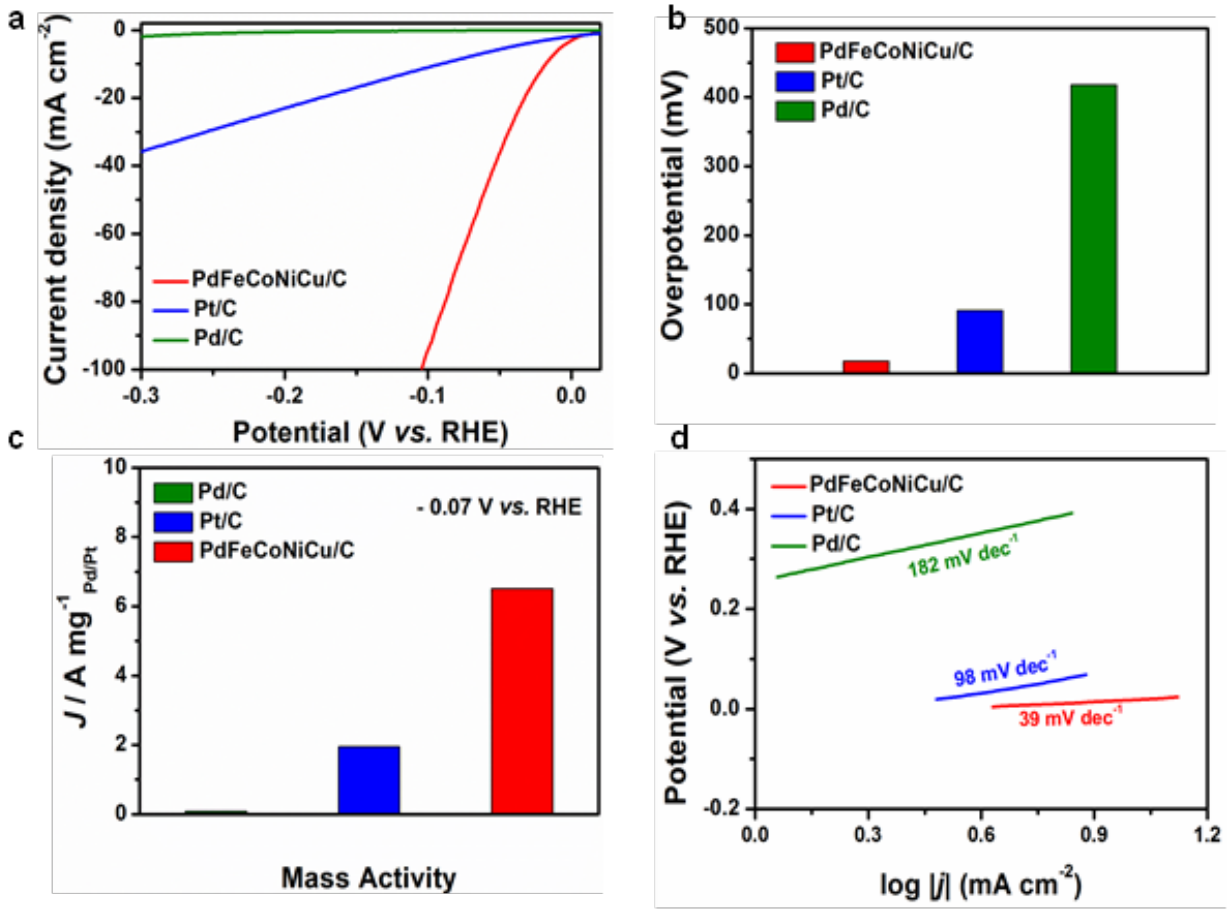


**Fig. 2** (a) HER polarization curves, (b) overpotential at 10 mA cm-2, (c) mass activity at −0.07 V vs. RHE. (d) Tafel slope of the PdFeCoNiCu/C, Pt/C and Pd/C in 1.0 M KOH solution.

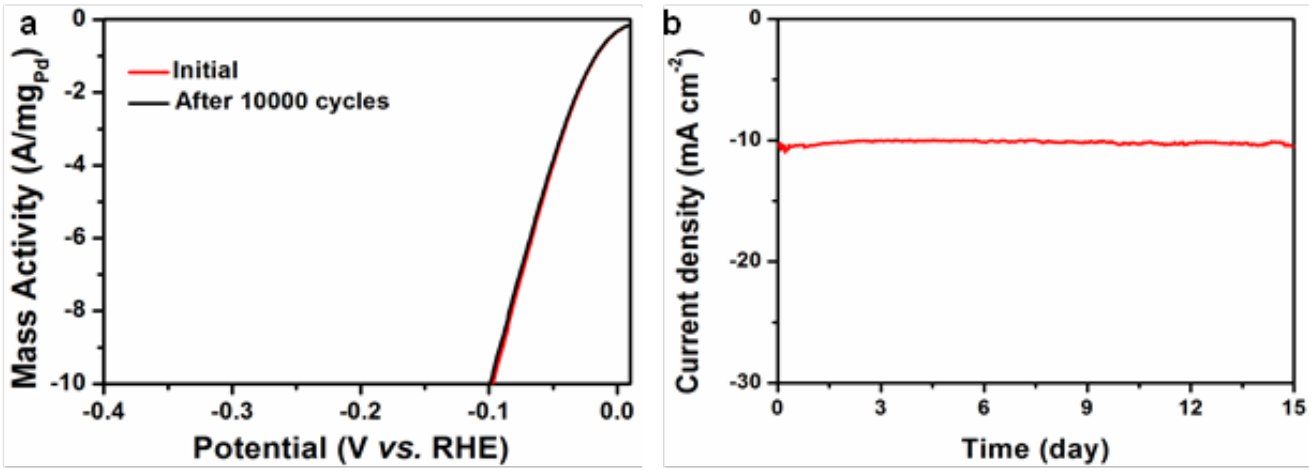


**Fig. 3** (a) HER polarization curves of PdFeCoNiCu/C before and after 10000 CV cycles. (b) Galvanostatic measurement result of FeCoNiCu/C for HER at 18 mV.

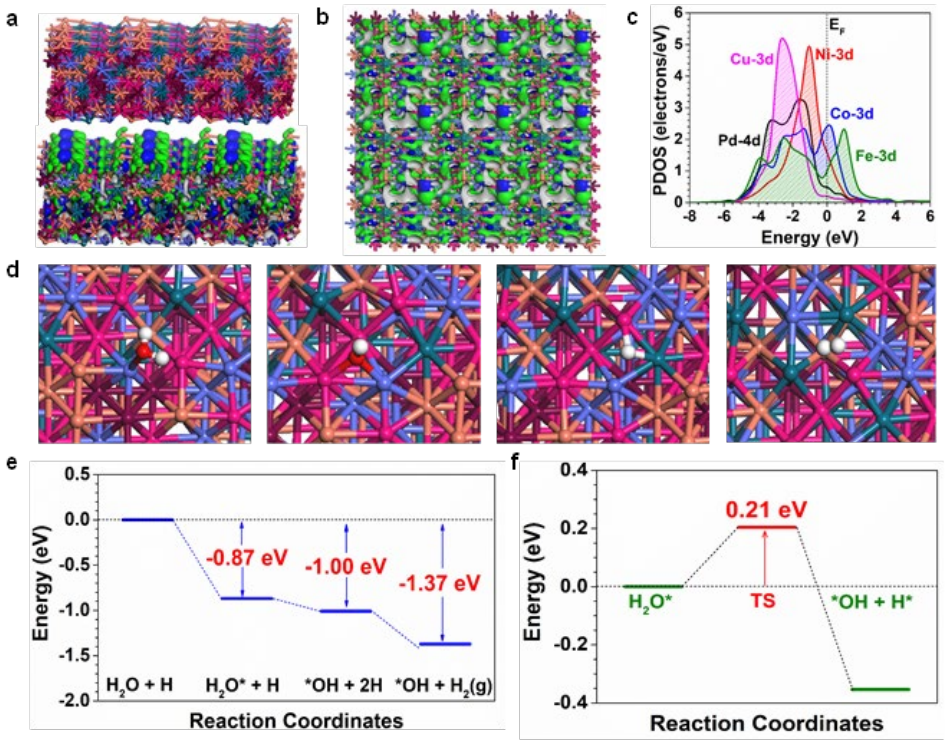


**Fig.4** (a) The side view of structure configuration and the real spatial contour plots for bonding and anti-bonding orbitals near EF for the HEA. Dark green balls = Pd; Brown balls= Fe; Blue balls = Co; Red balls = Ni and Orange balls = Cu. (b) The top view of the real spatial contour plots for bonding and anti-bonding orbitals near EF for the HEA. (c) The PDOSs of the HEA surface. (d) The most stable structural configuration of the reactants and key intermediates adsorptions. (e) The energetic pathway of HER under alkaline conditions. (f) The activation barrier of water splitting in HEA.